

Charge Neutral Two-Flavor Quark Matter in the Instanton Vacuum and Compact Stars

Hiyoshi KIUCHI and Makoto OKA

Department of Physics, Tokyo Institute of Technology, Tokyo 152-8551, Japan

(Received November 14, 2005)

Two-flavor (up and down) quark matter in the instanton vacuum is investigated using a mean-field approximation at $T = 0$. Electric charge neutrality is imposed for β -equilibrated quark matter. At finite chemical potential, a new charge neutral mixed phase is found between the chiral symmetry broken (CC) phase and the 2-flavor color superconducting (2SC) phase. The mixed phase is a mixture of a negatively charged CC subphase and a positively charged 2SC subphase with the appropriate volume ratio in a uniform electron gas. In addition, particle number densities, the effect of a finite current quark mass on the phase structure, the quark matter equation of state and compact stars are also investigated in this model.

§1. Introduction

Recent progress in mapping the QCD phase diagram has revealed that quark matter at low temperature has a rich phase structure, including a two-flavor color superconducting (2SC) phase and a color-flavor locking (CFL) phase.^{1)–3)} We conjecture that such quark matter exists inside compact stars.^{4),5)} Quark matter inside a compact star should be neutral with respect to electric as well as color charge. In particular, electric charge neutrality is necessary in order for the star to be held together by the gravitational force.⁶⁾ Furthermore, quark matter in compact stars is believed to be in β -equilibrium; that is, β -processes, such as ($d \rightarrow u + e^- + \bar{\nu}_e$, $u + e^- \rightarrow d + \nu_e$), should proceed with an equal rate in the opposite direction. As a result, when neutrinos are untrapped, the chemical potentials of the up quark (μ_u), down quark (μ_d) and electron (μ_e) satisfy the relation $\mu_d = \mu_u + \mu_e$.^{7),8)}

To this time, many studies have investigated charge neutral quark matter. In some of them, NJL-type models are used. In these studies, the possibility of the appearance of new phases, such as the gapless 2SC phase, the gapless CFL phase and mixed phases is discussed.^{9)–16),18)} In Ref. 10), in addition to the ordinary 2SC_{ud}, CFL and normal quark matter (NQ) phases, the realizability of exotic 2SC phases, such as 2SC_{us}, 2SC_{ds} and 2SC_{us+ds}, is studied. There can exist nine types of mixed phases, which are constructed from the NQ, 2SC_{ud}, CFL and the above-mentioned exotic 2SC phases. Phase mixing exists for quark chemical potentials, μ , in the range $\mu = 340.9$ MeV– $\mu = 465.7$ MeV. Mixing between the NQ and 2SC_{ud} phases is that which appears for the smallest values of μ and mixing between the 2SC_{us} and CFL phases is that which appears for the largest values. Some compact stars that correspond to the quark matter equations of states in the NJL-type models have reasonable radii and masses.^{11),19)} Furthermore, in a simple phenomenological bag model study, it was found that hybrid stars with quark matter cores and nuclear

matter surfaces can masquerade as neutron stars.²⁰⁾

For a compact star, relevant values of the baryon chemical potential ($\mu_B = 3\mu$) lie in low to intermediate region ($\mu < 0.5$ GeV, the density might be as large as $10\rho_0$, where $\rho_0 \sim 0.46 \text{ fm}^{-3}$).⁵⁾ Within the region at low temperature, an instanton induced nonperturbative interaction, whose dependence on the quark chemical potential μ is significant, is important for quark-antiquark ($\bar{q}q$) and quark-quark (qq) interactions.^{21),22)}

The aim of this paper is to explore relevant phases of neutral quark matter under the influence of the instanton-induced interaction (III). There have been some reports concerning quark matter in the instanton vacuum without the charge neutrality condition.^{23),24)} In these studies, the quark zero-mode eigenstate, which is the ground state of the quark in the instanton vacuum, is not fully taken into account in the interaction. In particular, the μ dependence of the interaction is completely ignored. In addition, the fact that the instanton-induced interaction is originally a pre-exponential factor in the partition function is ignored.²⁵⁾

Carter and Diakonov used approximated μ -dependent form factors (μ -FF) that arise from the μ -dependent quark zero mode function.²¹⁾ They found that the introduction of the μ -FF has an important effect. In return for raising the interaction term into the exponent, we have an additional term (L_{add}) and a constraint on the strength of the quark-quark and quark-antiquark effective interactions. As a consequence, in the instanton vacuum, the effective coupling strength between fermions is inevitably μ -dependent and related to the instanton density and to the order parameters. Carter and Diakonov determined the μ -dependent coupling strength by fixing the average instanton size $\bar{\rho}$ and assuming that the instanton density does not change as long as the quark chemical potential is below $\bar{\rho}^{-1} \sim 600$ MeV. We employ the same strategy in the present study.

However, we make some important improvements in the model developed by Carter and Diakonov in Ref. 21). First, we make use of the full μ -dependent form factor instead of the approximated one. In addition, the thermodynamic potential in our model contains the complete contributions of the one-loop diagrams, while that used by Carter and Diakonov does not. We find that the introduction of μ -FF requires both the L_{add} and the constraint on the effective coupling strength for inducing the chiral phase transition. Furthermore it is noteworthy that our improvements enable us to investigate systems under compact star constraints (namely, charge neutrality and β -equilibrium), because we can distinguish μ_u from μ_d in the partition function, including the interaction part. In the numerical calculations, we set the values of the instanton density $\frac{N}{V}$ and the average instanton size $\bar{\rho}$ on the basis of the lattice QCD calculation and the instanton liquid model calculation.^{26),27)} Accordingly, there is no free parameter in the present model.

For compact star phenomenology, the 2SC phase can be more important than CFL phase. Because the latter requires approximate flavor $SU(3)$ symmetry, the relevant region is $\mu > 450$ MeV, which is of the order of the strange quark mass, whereas at the center of a typical compact star, μ is believed to be no larger than 500 MeV.⁴⁾ As shown below, the mixed phase and the 2SC phase already appear

at $\mu = 293$ and 320 MeV, respectively, in our model. Therefore, we employ the instanton-induced interaction as the effective interaction, which is attractive for both $\bar{q}q$ and qq pairing and restrict our study to $N_f = 2$, corresponding to a system of up and down quarks.^{21), 22)}

The outline of the paper is as follows. In §2, we give a brief introduction for the μ -dependent instanton-induced interaction (μ -III). Then, we derive the partition function based on μ -III and obtain a constraint on the effective coupling strength. In §3, we derive the thermodynamic potential (Ω) in the mean-field approximation and, at the same time, we obtain the gap equation. In §4, we derive the electric charge neutrality condition in this model. In §5, we calculate several thermodynamic quantities and present the numerical results. In §6, we evaluate the charge neutral quark matter equation of state. In §7, we estimate the finite current quark mass effect on the phase structure. In §8, the sequence of compact stars predicted by this model is investigated. Section 9 is devoted to conclusions.

§2. Instanton-induced interaction

In the instanton vacuum the massless or nearly massless quark propagation takes place mainly through the 't Hooft zero mode $\Psi_{(0)}(x, \mu)$.^{25), 28)} The propagator can be approximated as

$$\langle 0|T\Psi(x)\bar{\Psi}(y)|0\rangle \sim \Psi_{(0)}(x, \mu)\Psi_{(0)}^\dagger(y, -\mu). \quad (2.1)$$

Then the effective Lagrangian, L_{inst} , for two flavors at finite μ is expressed in the momentum space as²²⁾

$$\begin{aligned} L_{\text{inst}} = & \int \frac{d^4p d^4p' d^4k d^4k'}{(2\pi)^{16}} \frac{1}{16N_c(N_c^2 - 1)} \left(N_c \delta_{\alpha_1}^{\beta_1} \delta_{\alpha_2}^{\beta_2} - \delta_{\alpha_2}^{\beta_1} \delta_{\alpha_1}^{\beta_2} \right) \epsilon^{st} \\ & \times \bar{\Psi}_1^{\alpha_1}(p') G(p', \mu) \frac{1 + \gamma_5}{2} G^\dagger(p, -\mu) \Psi_s^{\beta_1}(p) \\ & \times \bar{\Psi}_2^{\alpha_2}(k') G(k', \mu) \frac{1 + \gamma_5}{2} G^\dagger(k, -\mu) \Psi_t^{\beta_2}(k) \\ & \times (2\pi)^4 \delta^4(p' + k' - p - k) \\ & + \text{h.c.}, \end{aligned} \quad (2.2)$$

where $\alpha_1, \alpha_2, \beta_1$ and β_2 denote color indices and $1, 2, s$ and t denote flavor indices. The functions G and G^\dagger here are the form factors, defined by

$$G(p, \mu) \equiv (p_\xi \gamma^\xi) [\phi_\nu(p, \mu) \gamma^\nu], \quad (2.3)$$

where

$$\phi_\nu(p, \mu) \equiv [p_1 \phi(|\mathbf{p}|, p_4, \mu), p_2 \phi(|\mathbf{p}|, p_4, \mu), p_3 \phi(|\mathbf{p}|, p_4, \mu), \phi_4(|\mathbf{p}|, p_4, \mu)] \quad (2.4)$$

are the Fourier components of the quark zero eigen-mode at non-zero μ (see Appendix A).²¹⁾

The instanton-induced interaction L_{inst} is the sum of the individual instanton (I) and anti-instanton (\bar{I}) contributions :

$$L_{\text{inst}} = L_I + L_{\bar{I}}. \quad (2.5)$$

The effective Lagrangian terms L_I and $L_{\bar{I}}$ are originally pre-exponential factors in the partition function Z in the path-integral formalism.^{21),25)}

$$Z = \int D\bar{\Psi}D\Psi \exp \left[\int d^4x \{ \bar{\Psi}(i\cancel{\partial} - i\mu\gamma_4 - m)\Psi \} \right] (L_I)^{N_I} (L_{\bar{I}})^{N_{\bar{I}}}. \quad (2.6)$$

Here, m represents the current quark mass, and N_I and $N_{\bar{I}}$ are the instanton and anti-instanton numbers, respectively.

In order to raise the operators L_I and $L_{\bar{I}}$ into the exponent, we use the inverse Laplace transformation.²¹⁾ We introduce the undetermined multipliers λ_I and $\lambda_{\bar{I}}$, which play the role of the coupling strength, as clarified below. Then we can write

$$Z = \int d\lambda_I d\lambda_{\bar{I}} Z(\lambda_I, \lambda_{\bar{I}}), \quad (2.7)$$

where

$$\begin{aligned} Z(\lambda_I, \lambda_{\bar{I}}) \equiv & \int D\bar{\Psi}D\Psi \exp \left[\int d^4x \{ \bar{\Psi}(i\cancel{\partial} - i\mu\gamma_4 - m)\Psi \} \right. \\ & + \lambda_I L_I + N_I \left\{ \log \left(\frac{N_I}{\lambda_I V} \right) - 1 \right\} \\ & \left. + \lambda_{\bar{I}} L_{\bar{I}} + N_{\bar{I}} \left\{ \log \left(\frac{N_{\bar{I}}}{\lambda_{\bar{I}} V} \right) - 1 \right\} \right], \quad (2.8) \end{aligned}$$

with V the four-dimensional volume.

In this study, we assume the CP invariant case of the $\theta = 0$ instanton theta vacuum. In this case, it was found in an instanton gas model study that the dominant instanton-anti-instanton configuration is that for which²⁹⁾

$$N_I = N_{\bar{I}} = \frac{N}{2}, \quad (2.9)$$

and hence,

$$\lambda_I = \lambda_{\bar{I}} = \lambda. \quad (2.10)$$

Then the partition function Z reduces to

$$Z = \int d\lambda \int D\bar{\Psi}D\Psi \exp \left[\int d^4x \{ \bar{\Psi}(i\cancel{\partial} - i\mu\gamma_4 - m)\Psi \} + \lambda L_{\text{inst}} + L_{\text{add}} \right], \quad (2.11)$$

where

$$L_{\text{add}} \equiv N \left\{ \log \left(\frac{N}{2\lambda V} \right) - 1 \right\}. \quad (2.12)$$

Next, applying the saddle point method in the thermodynamic limit ($N, V \rightarrow +\infty$ with N/V fixed), we recover Eq. (2.6) exactly.²¹⁾ Here, the multiplier λ is determined by the condition

$$\frac{\delta \log Z(\lambda)}{\delta \lambda} = 0 \tag{2.13}$$

as

$$\frac{N}{V} = \frac{\lambda \langle L_{\text{inst}} \rangle}{V}, \tag{2.14}$$

where $\langle \dots \rangle$ represents the expectation value. The above equation can be naturally understood if one thinks of the instanton density as being the amplitude of the vacuum to vacuum transition in the presence of the instanton.

§3. Thermodynamic potential in the mean-field approximation

Utilizing Fierz rearrangements, we decompose L_{inst} into two parts, one containing only the color singlet (1_c) quark bilinears and the other containing only the color antitriplet ($\bar{3}_c$) bilinears.²¹⁾ In addition, we introduce two kinds of mean fields, σ and Δ , which are the order parameters of the chiral and color symmetry breaking, respectively:

$$\text{dynamically generated quark mass : } \sigma = -2K \langle \bar{\Psi} \Psi \rangle, \tag{3.1}$$

$$\text{diquark energy gap : } \Delta = -2K' \langle \bar{\Psi}_\alpha C \gamma_5 \Psi_\beta \rangle \epsilon^{\alpha\beta 3}. \tag{3.2}$$

Here, the color indices α and β run from 1 to 2. According to the Fierz rearrangements, the effective coupling strengths K and K' are proportional to λ and are related as $K' = 0.75K$. In the chiral limit, the dynamically generated quark mass is equal to the constituent quark mass.

Because the diquark condensates are composed of quarks of colors 1 and 2, do not contain quarks of color 3, a non-zero Δ breaks the color $SU(3)$ symmetry down to the color $SU(2)$ symmetry.

When the chemical potential of up quarks (μ_u) is different from that of down quarks (μ_d), the partition function (Z_{eff}) is given by

$$Z_{\text{eff}} = \int D\bar{\Psi} D\Psi \exp(-S), \tag{3.3}$$

where the corresponding action S is given by

$$S = S_1 + S_2 + S_3, \tag{3.4}$$

$$S_1 = V \left[\frac{\sigma^2}{4K} + \frac{\Delta^2}{4K'} \right], \tag{3.5}$$

$$S_2 = \int \frac{d^4p}{(2\pi)^4} \left[\bar{\Psi}_{\alpha,u}(p) \{ \not{p} + i\mu_u \gamma_4 + M_u \} \Psi_u^\alpha(p) \right. \\ \left. + \bar{\Psi}_{\alpha,d}(p) \{ \not{p} + i\mu_d \gamma_4 + M_d \} \Psi_d^\alpha(p) \right]$$

$$\begin{aligned}
& + \frac{1}{2} \left\{ \Psi_u^{\alpha T}(-p) \Gamma(-p, \bar{\mu}) \Psi_d^\beta(p) - \Psi_d^{\alpha T}(-p) \Gamma(-p, \bar{\mu}) \Psi_u^\beta(p) \right. \\
& \left. + \bar{\Psi}_u^\alpha(p) \Gamma^\dagger(p, \bar{\mu}) \bar{\Psi}_d^{\beta T}(-p) - \bar{\Psi}_d^\alpha(p) \Gamma^\dagger(p, \bar{\mu}) \bar{\Psi}_u^{\beta T}(-p) \right\} \epsilon_{\alpha\beta 3}, \quad (3.6)
\end{aligned}$$

$$S_3 = -L_{\text{add}} = -N \left[\log \left(\frac{N}{2\lambda V} \right) - 1 \right], \quad (3.7)$$

where α and β are color indices, $\bar{\mu} [\equiv (\mu_u + \mu_d)/2]$ is the average chemical potential for the color-antitriplet pairs, and we have

$$M_u \equiv m_u + M(p, \mu_u), \quad (3.8)$$

$$M_d \equiv m_d + M(p, \mu_d), \quad (3.9)$$

$$\Gamma(p, \bar{\mu}) \equiv \Delta^* G(p, \bar{\mu}) C^\dagger \gamma_5 G^T(-p, \bar{\mu}). \quad (3.10)$$

Here, the function $M(p, \mu)$ is a momentum dependent dynamically generated quark mass:

$$M(p, \mu) \equiv \sigma G(p, \mu) G^\dagger(p, \mu). \quad (3.11)$$

The explicit expressions of the form factors are as follows: For a color-singlet pair, we have

$$G(p, \mu) G^\dagger(p, \mu) = (p + i\mu)_\eta (p + i\mu)_\eta \phi_\nu(p, \mu) \phi_\nu(p, \mu), \quad (3.12)$$

while for a color-antitriplet pair we have

$$G(p, \mu) C^\dagger \gamma_5 G^T(-p, \mu) C^\dagger \gamma_5 = A(p, \mu) + B(p, \mu), \quad (3.13)$$

where

$$\begin{aligned}
A(p, \mu) \equiv & \mathbf{p} \cdot \boldsymbol{\gamma} \gamma_4 \left\{ i 2\mu \phi_\nu(p, \mu) \phi_\nu^*(p, \mu) \right. \\
& \left. - (p^2 + \mu^2) [\phi_4(p, \mu) \phi_4^*(p, \mu) - \phi_4^*(p, \mu) \phi_4(p, \mu)] \right\}, \quad (3.14)
\end{aligned}$$

$$\begin{aligned}
B(p, \mu) \equiv & (p^2 + \mu^2) \phi_\nu(p, \mu) \phi_\nu(-p, \mu) \\
& + (p + i\mu)_\eta \phi_\eta(p, \mu) (p - i\mu)_\nu \phi_\nu(-p, \mu) \\
& - (p + i\mu)_\eta \phi_\eta(-p, \mu) (p - i\mu)_\nu \phi_\nu(p, \mu). \quad (3.15)
\end{aligned}$$

In the mean-field approximation, the constraint on the effective coupling strengths K and K' Eq. (2.14) is expressed explicitly in terms of σ and Δ as²²⁾

$$\frac{N}{V} = \frac{\sigma^2}{4K} + \frac{\Delta^2}{4K'}. \quad (3.16)$$

After integrating out the quark fields $\bar{\Psi}$ and Ψ in the partition function Z_{eff} , we obtain

$$Z_{\text{eff}} = \exp(-S_{\text{eff}}). \quad (3.17)$$

The corresponding effective action S_{eff} is given by

$$S_{\text{eff}} = V \left\{ \frac{\sigma^2}{4K} + \frac{\Delta^2}{4K'} + (2 - N_c) \int \frac{d^4p}{(2\pi)^4} \log(YY^*) - 2 \int \frac{d^4p}{(2\pi)^4} \log(FF^*) \right\} - N \left[\log \left(\frac{N}{2\lambda V} \right) - 1 \right], \quad (3.18)$$

where

$$Y \equiv \{ |\mathbf{p}|^2 + (p_4 + i\mu_u)^2 + M_u^2 \} \{ |\mathbf{p}|^2 + (p_4 - i\mu_d)^2 + M_d^2 \}, \quad (3.19)$$

$$F \equiv Y + 2\Delta^2(M_u M_d^* W + U) + \Delta^4 W^2, \quad (3.20)$$

$$W \equiv \{ |\mathbf{p}|^2 + (p_4 + i\bar{\mu})^2 \} [(\phi_\nu \phi_\nu^*)^2 - 4|\mathbf{p}|^2 \text{Im}^2(\phi\phi_4^*)], \quad (3.21)$$

$$\begin{aligned} U \equiv & (p^2 + \mu_u \mu_d) \left[\{ (p^2 + \bar{\mu}^2)^2 + 4\bar{\mu}^2 |\mathbf{p}|^2 \} \{ (\phi_\nu \phi_\nu^*)^2 + 4|\mathbf{p}|^2 \text{Im}^2(\phi\phi_4^*) \} \right. \\ & \left. + 16\bar{\mu} |\mathbf{p}|^2 (p^2 + \bar{\mu}^2) (\phi_\nu \phi_\nu^*) \text{Im}(\phi\phi_4^*) \right] - 4|\mathbf{p}|^2 (\mu_u + \mu_d) \left[\bar{\mu} (p^2 + \bar{\mu}^2) (\phi_\nu \phi_\nu^*)^2 \right. \\ & \left. + \{ (p^2 + \bar{\mu}^2)^2 + 4\bar{\mu}^2 |\mathbf{p}|^2 \} (\phi_\nu \phi_\nu^*) \text{Im}(\phi\phi_4^*) + 4\bar{\mu} |\mathbf{p}|^2 (p^2 + \bar{\mu}^2) \text{Im}^2(\phi\phi_4^*) \right] \\ & + ip_4 (\mu_u - \mu_d) \left[\{ (p^2 + \bar{\mu}^2)^2 + 4\bar{\mu}^2 |\mathbf{p}|^2 \} \{ (\phi_\nu \phi_\nu^*)^2 + 4|\mathbf{p}|^2 \text{Im}^2(\phi\phi_4^*) \} \right. \\ & \left. + 16\bar{\mu} |\mathbf{p}|^2 (p^2 + \bar{\mu}^2) (\phi_\nu \phi_\nu^*) \text{Im}(\phi\phi_4^*) \right], \end{aligned} \quad (3.22)$$

$$p^2 \equiv |\mathbf{p}|^2 + p_4^2. \quad (3.23)$$

The mean fields (σ, Δ) and the μ -dependent effective coupling strength K (K') are determined simultaneously from the following coupled gap equation with the constraint Eq. (3.16):

$$\frac{\delta S_{\text{eff}}}{\delta \sigma} \Big|_{\text{fixed } K} = \frac{\delta S_{\text{eff}}}{\delta \Delta} \Big|_{\text{fixed } K} = 0. \quad (3.24)$$

Finally we obtain the thermodynamic potential in the mean-field approximation Ω , which consists of Ω_q , the contribution of the quark sector, and Ω_e , that of electrons (assumed to be massless):

$$\Omega = \Omega_q + \Omega_e, \quad (3.25)$$

where

$$\Omega_q = \frac{S_{\text{eff}}}{V}, \quad (3.26)$$

$$\Omega_e = 2 \int_0^{\mu_e} \frac{d^3p}{(2\pi)^3} (p - \mu_e) = -\frac{\mu_e^4}{12\pi^2}. \quad (3.27)$$

§4. Charge neutrality condition

Quark matter in a compact star is believed to be in β -equilibrium and charge-neutral.^{6),7)} When neutrinos are untrapped, the chemical potentials of quarks and electrons are related as

$$\mu_d = \mu_u + \mu_e. \quad (4.1)$$

We estimate the following four kinds of densities of the system.

(I) The electric charge density Q ,

$$Q = \frac{2}{3}n_u - \frac{1}{3}n_d - n_e, \quad (4.2)$$

where n_u , n_d and n_e denote the particle number densities of the up quark, down quark and electron, respectively.

(II) The color charge densities Q_3 and Q_8 ,

$$Q_3 = \frac{1}{2} \sum_{u,d} (n_1 - n_2), \quad (4.3)$$

$$Q_8 = \frac{1}{3} \sum_{u,d} (n_1 + n_2 - 2n_3). \quad (4.4)$$

(III) The baryon number density Q_B ,

$$Q_B = \frac{1}{3} \sum_{u,d} (n_1 + n_2 + n_3), \quad (4.5)$$

where the subscripts 1,2 and 3 indicate the colors.

The number densities on the right-hand sides of the above four equations are determined by derivatives of the thermodynamic potential Ω with respect to the corresponding chemical potentials μ_j as follows:

$$n_j = -\frac{\partial \Omega}{\partial \mu_j}. \quad (4.6)$$

In the 2SC phase, color $SU(2)$ symmetry, which consists of the colors 1 and 2, remains intact. Consequently, one of the color charges, Q_3 , remains zero, while the other color charge, Q_8 , generally has a finite value in the 2SC phase without the charge neutrality condition.

In this study, in the differentiation of Ω with respect to μ_j , we ignore the μ_j -dependence of the form factors for simplicity.

In order to calculate the three kinds of charge densities, based upon Eq. (4.1) and (4.6), we choose the quark chemical potential as

$$\mu_{i,j}^{\alpha,\beta} = (\mu \delta_{i,j} - \mu_e Q_{i,j}) \delta^{\alpha,\beta} + \frac{1}{\sqrt{3}} \mu_8 \delta_{i,j} (\lambda_8)^{\alpha,\beta}, \quad (4.7)$$

where $\mu = \frac{\mu_B}{3}$, i and j are flavor indices, and α and β are color indices. The matrices Q and λ_8 are defined as $Q_{i,j} = \text{diag} \left(\frac{2}{3}, -\frac{1}{3} \right)$ and $(\lambda_8)^{\alpha,\beta} = \text{diag} \left(\frac{1}{\sqrt{3}}, \frac{1}{\sqrt{3}}, -\frac{2}{\sqrt{3}} \right)$.

The values of μ_8 that satisfy the color charge neutrality condition in the 2SC phase are reported to be -10 MeV,^{9),30)} while the values of μ_u , μ_d and μ_e are larger than about 150 MeV. In this study, because μ_8 is small compared to μ_u , μ_d and μ_e , we set $\mu_8 = 0$.^{11),14)} Then μ_u and μ_d become independent of color and reduce to the

following forms:

$$\mu_u = \mu - \frac{2}{3}\mu_e, \quad (4.8)$$

$$\mu_d = \mu + \frac{1}{3}\mu_e. \quad (4.9)$$

The local electric charge neutrality condition is expressed as follows:

$$Q = -\frac{\partial\Omega}{\partial\mu_e} = 0. \quad (4.10)$$

§5. Charge neutral phase structure in the chiral limit ($m \rightarrow 0$) at $T = 0$

In this study we identify three phases that are realized in our model, the pure chiral condensate phase (CC : $\sigma \neq 0$ but $\Delta = 0$), the pure diquark condensate phase (2SC : $\sigma = 0$ but $\Delta \neq 0$) and the mixed phase (MX), which is a mixture of the CC and 2SC subphases.

5.1. Gap equation solutions that satisfy the electric charge neutrality condition

In this subsection we solve the gap equation Eq. (3.24) and the charge neutrality condition Eq. (4.10) with the help of the constraint on $K(K')$ given in Eq. (3.16) and report the results of our numerical computation of the thermodynamic potential. For the numerical calculation, we employed the value of the gluon condensate obtained from the lattice QCD calculation for the instanton density $\frac{N}{V}$ and set it to $(0.2 \text{ GeV})^4$.²⁶⁾ For the average instanton size $\bar{\rho}$, we adopt the result $\bar{\rho}(N/V)^{\frac{1}{4}} = \frac{1}{3}$ from the instanton liquid model calculation and set it to $\frac{1}{3} \text{ fm}$.²⁷⁾ Then, we obtain a constituent quark mass σ of 347 MeV and a chiral condensate $\langle\bar{\Psi}\Psi\rangle$ of $(-251 \text{ MeV})^3$ at $\mu = T = 0$. In addition, the bag pressure (B) appears as the difference between the pressures of the CC and virtual NQ ($\sigma = \Delta = 0$) phases. We have $B^{\frac{1}{4}} \sim 0.25 \text{ GeV}$ at $\mu = T = 0$. It should be noted that in the μ -III model, there is no free parameter.

Our main assumption is that the instanton density does not change when we increase the baryon chemical potential. This assumption is justified in the relevant region of μ_B for quark matter inside compact stars, according to the instanton liquid model calculation.³¹⁾

Figure 1 plots the thermodynamic potentials (Ω) as functions of μ ($= \frac{1}{3}\mu_B$) in the chiral limit, based on our numerical results. It is seen that the 2SC curve intersects the CC curve at $\mu = 312 \text{ MeV}$. At this point, the values of μ_e in the CC phase and the 2SC phase are 52 MeV and 211 MeV, respectively.

Figure 2 displays a close-up view near the intersection in Fig. 1. It is seen that a mixed phase is realized between $\mu = 293 \text{ MeV}$ and 320 MeV . However, unlike in the flavor symmetric case,²²⁾ a doubly symmetry broken phase, in which both chiral and color symmetries are broken, is not realized, because of the local electric charge neutrality condition.

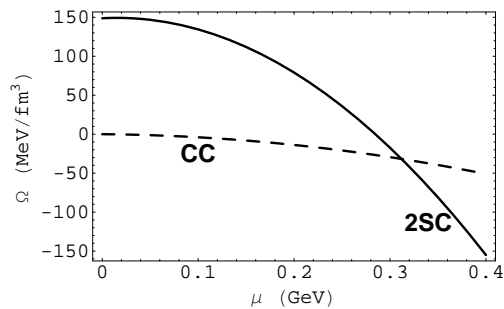


Fig. 1. Dependence of Ω on the quark chemical potential ($\mu = \frac{\mu_B}{3}$). The 2SC curve intersects the CC curve at $\mu = 312$ MeV.

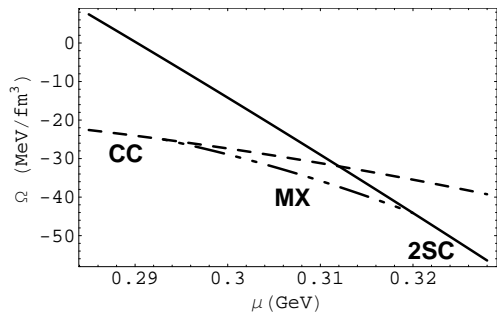


Fig. 2. A close-up view near the intersection. The MX phase is realized in the region where the quark chemical potentials (μ) are between 293 MeV and 320 MeV.

In the 2SC phase the values of K' and Δ are $K' = 18.2 \text{ GeV}^{-2}$ and $\Delta = 0.34 \text{ GeV}$ at $\mu = 0.32 \text{ GeV}$ and $K' = 13.1 \text{ GeV}^{-2}$ and $\Delta = 0.29 \text{ GeV}$ at $\mu = 0.4 \text{ GeV}$. The values of K' and Δ decrease as μ increases. Thus, the value of the effective coupling strength K' is large compared to that in the NJL-type models, as long as μ is not too large. The value of Δ in the present model is a few times larger than that in the NJL-type models, but it is comparable to the results obtained in Ref. 21), in which μ -III is also used as the effective interaction for two-flavor quark matter. The large value of Δ is considered to be a result of the strong coupling strength for a color anti-triplet bilinear in the μ -III models.

5.2. Mixed phase construction

A globally charge neutral mixed phase can be constructed from a mixture of two oppositely charged subphases with an appropriate volume ratio. The subphases in the mixed phase have to have the same values of μ , μ_e and Ω (the Gibbs phase equilibrium condition).

Figure 3 plots the dependences of the electric charge densities (Q_{CC} and Q_{2SC}) on μ_e at $\mu = 0.31 \text{ GeV}$. It is seen that at low μ_e both the subphases are positively charged, while at the endpoints ($\mu_e = 0.15 \text{ GeV}$), the 2SC subphase is still positively charged, but the CC subphase is negatively charged. The pressures in both the subphases are equal only at the endpoints.

Figure 4 displays the dependences of Q_{CC} and Q_{2SC} on μ . At each μ , the two subphases have the same values of μ_e and the pressure ($P = -\Omega$). It is seen that the CC subphase is negatively charged, while the 2SC subphase is positively charged.

For bulk charge neutrality the volume fraction that must be occupied by the 2SC subphase is given by

$$\chi = \frac{Q_{CC}}{Q_{CC} - Q_{2SC}}. \quad (5.1)$$

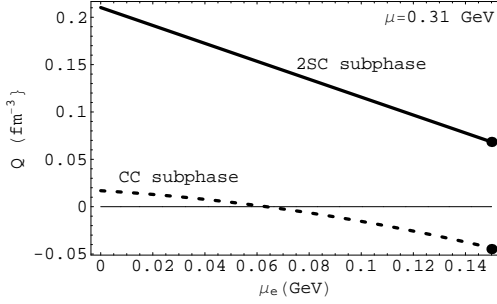


Fig. 3. Dependences of the electric charge densities (Q_{CC} and Q_{2SC}) on μ_e at $\mu=0.31$ GeV. The values of Ω in the CC and 2SC subphases become equal at the end points ($\mu_e=0.15$ GeV).

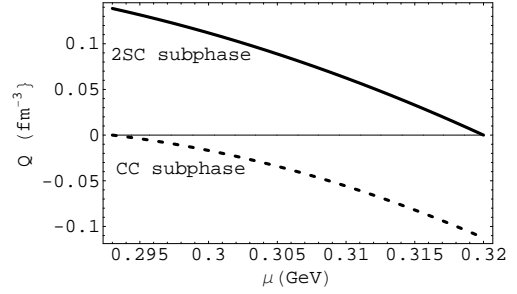


Fig. 4. Dependences of Q_{CC} and Q_{2SC} on μ . At each μ , the two subphases have the same values of Ω and μ_e .

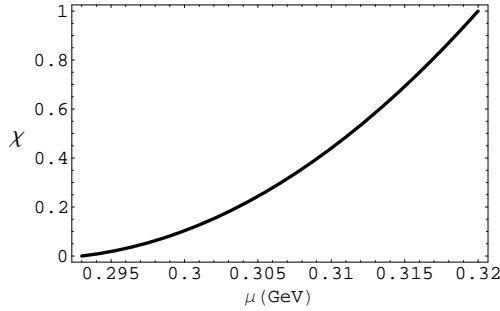


Fig. 5. Volume fraction χ of the 2SC subphase for global charge neutrality.

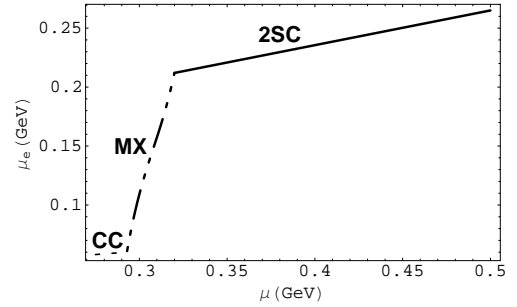


Fig. 6. μ vs μ_e . The value of μ_e increases steeply in the mixed phase as μ increases.

Therefore, we have

$$Q = (1 - \chi)Q_{CC} + \chi Q_{2SC} = 0. \quad (5.2)$$

As shown in Fig. 5, the volume fraction of the 2SC subphase increases monotonically from zero to unity.

Figure 6 plots the dependence of μ_e on μ . It is seen that μ_e increases steeply in the mixed phase as μ increases.

It is noteworthy that in this model, the MX phase is the only route between the locally charge neutral CC and 2SC phases that is compatible with the Gibbs condition.

5.3. Particle number densities

In the mixed phase the number density n_j of the particle species j is given by the volume-weighted average of the individual particle densities:

$$n_j = (1 - \chi)n_j^{CC} + \chi n_j^{2SC}. \quad (5.3)$$

Figures 7 and 8 display the particle number densities. It is seen that the densities of up and down quarks increase steeply in the mixed region as μ increases. Accord-

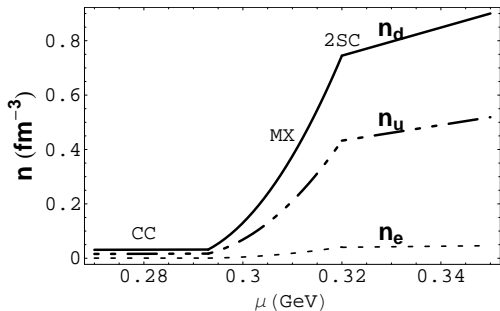


Fig. 7. The mixed region (MX) is narrow with respect to μ , but relatively wide with respect to n .

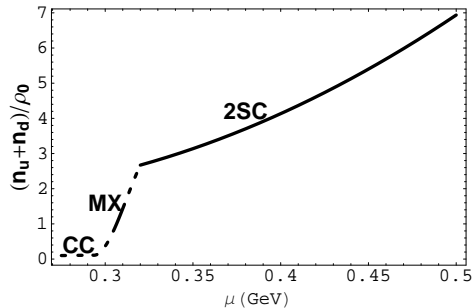


Fig. 8. The 2SC phase appears at $n_u + n_d = 2.67\rho_0$.

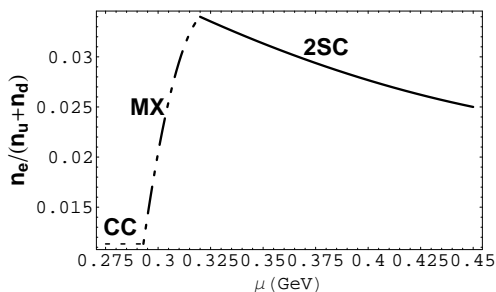


Fig. 9. In the CC phase, electric charge neutrality is almost realized without electrons.

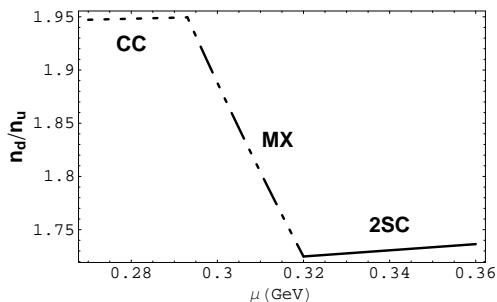


Fig. 10. In the CC phase, we have $n_d/n_u \sim 2$, which is almost equal to the ratio in neutron matter.

ingly, we find that the mixed region is narrow with respect to μ , but relatively wide with respect to n_u and n_d .

Figures 9 and 10 reveal that, in the CC phase, electric charge neutrality is almost realized without electrons (Fig. 9); that is, the number of down quarks is twice that of up quarks (see Fig. 10). Thus, it is interesting that in the CC phase, the ratio n_d/n_u is almost the same as that in neutron matter.

5.4. Upper limit for the surface tension η , below which the mixed phase is favored

To this point, we have ignored the effects of the Coulomb force and the surface tension between different components in the mixed phase. These effects reduce the pressure in the mixed phase. As a consequence, the mixed phase is favored only if the surface tension is not too large. In this subsection, we estimate the upper limit on the surface tension η_{ul} , below which the mixed phase is favored over the locally charge-neutral phases.

The mixed phase can be structured so as to minimize the sum of the CC-2SC interface surface energy (E_S) and the Coulomb energy (E_C). Then the thermodynamic potential of the mixed phase Ω_{MX} , including the surface and Coulomb contributions,

Table I. The upper limit for the surface tension, η_{ul} .

μ (MeV)	η_{ul} (MeV/fm ²)
305	6.7
310	20.7
313	41.8
318	17.6

is given by³⁰⁾

$$\Omega_{MX} = \Omega + E_S + E_C. \tag{5.4}$$

Let us consider a crystalline structure consisting of Wigner-Seitz cells. In each cell, the region occupied by the smaller subphase must be surrounded by the larger subphase so that the total charge content of the cell is neutral. When the smaller subphase forms a droplet, the sum of the surface and Coulomb energies per unit volume (E_{tot}) is given by³²⁾⁻³⁴⁾

$$E_{tot} \equiv E_S + E_C = 6\pi x \left(\frac{9\eta^2 e^2 \Delta Q^2 f(x)}{16\pi^2} \right)^{\frac{1}{3}}, \tag{5.5}$$

where x denotes the volume fraction of the smaller subphase, and η represents the surface tension. Here we have assumed that the interface is thin in comparison with the radius of the Wigner-Seitz cell.

The quantity ΔQ is the difference between the charge densities of the two subphases:

$$\Delta Q \equiv Q_{2SC} - Q_{CC}, \tag{5.6}$$

and the geometrical factor $f(x)$ is given by

$$f(x) = \frac{2 + x - 3x^{\frac{1}{3}}}{5}. \tag{5.7}$$

When $\Delta\Omega \geq E_{tot}$ at a given μ , the mixed phase is possible. Here $\Delta\Omega$ denotes the difference between the thermodynamic potentials, which is given by

$$\Delta\Omega = \Omega_{CC} - \Omega : 293 \leq \mu \leq 312 \text{ MeV}, \tag{5.8}$$

$$\Delta\Omega = \Omega_{2SC} - \Omega : 312 \leq \mu \leq 320 \text{ MeV}. \tag{5.9}$$

Using Eqs. (5.4) and (5.5), we can calculate the upper limit on the surface tension η_{ul} , below which the mixed phase is favored:

$$\eta_{ul} = \frac{4}{3\sqrt{216\pi f(x)\Delta Q e}} \left(\frac{\Delta\Omega}{x} \right)^{\frac{3}{2}}. \tag{5.10}$$

The value of η_{ul} becomes large near the CC-2SC intersection point ($\mu = 312$ MeV).

Furthermore we estimate the radius of a droplet (ℓ) and the distance between centers ($2L$) at a given value of the surface tension. We find that at $(\mu, \eta) = (313$

MeV, 5 MeV/fm²), the values of ℓ and L are 10.8 fm and 15.3 fm, respectively. The electron Debye screening length, $\lambda_D = \left(-4\pi e^2 \frac{\partial^2 \Omega_e}{\partial \mu_e^2}\right)^{-\frac{1}{2}}$, at $\mu = 313$ MeV is about 13 fm, which is comparable to the radius of the Wigner-Seitz cell.³⁵⁾

§6. Equation of state

In this section we present the equation of state for charge-neutral two-flavor quark matter in the chiral limit in the pressure-energy density (P - E) plane.

The energy density can be calculated using Ω as

$$\begin{aligned} E &= -P + \mu_j n_j \\ &= \Omega - \mu_j \frac{\partial \Omega}{\partial \mu_j}. \end{aligned} \tag{6.1}$$

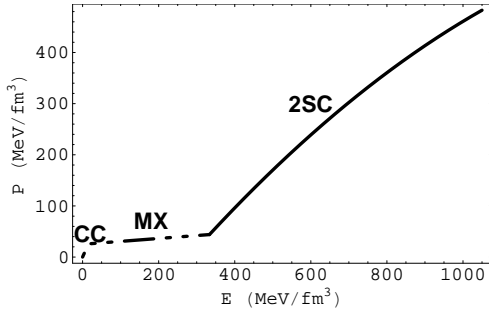


Fig. 11. Dependence of the pressure (P) as a function of the energy density (E) in the chiral limit at $T = 0$.

density in the chiral limit. The pressure in the MX phase changes from 26 MeV/fm³ to 44 MeV/fm³, while in 2SC phase, the pressure increases steeply as E increases. The region plotted in Fig. 11 corresponds to $0 \leq \mu < 600$ MeV, satisfying $\mu\bar{\rho} < 1$.

§7. Finite current quark mass effect

In the chiral limit, a mixed phase is realized between $\mu = 293$ MeV and 320 MeV (Fig. 2), while in the cases of $m_u = 5$ MeV and $m_d = 9$ MeV (see Fig. 12) and $m_u = m_d = 10$ MeV (see Fig. 13), the mixed phases are realized between $\mu = 312$ MeV and 350 MeV and between $\mu = 320$ MeV and 362 MeV, respectively. Thus, when we introduce a finite current quark mass, the mixed region shifts upward and becomes wider than that in the chiral limit.

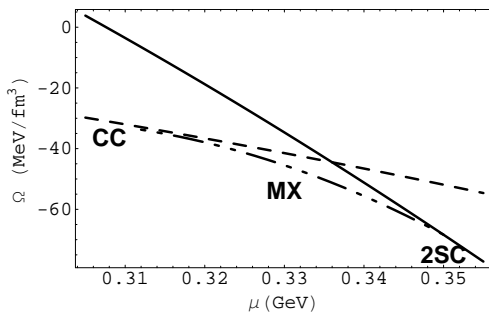


Fig. 12. Phase structure with $m_u = 5$ MeV and $m_d = 9$ MeV.

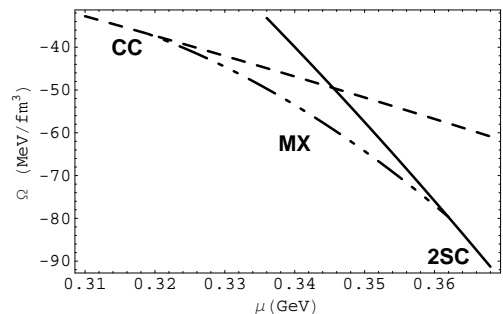


Fig. 13. Phase structure with $m_u = m_d = 10$ MeV.

The pressure in the mixed phase in the case $m_u = 5$ MeV and $m_d = 9$ MeV varies from 35 to 71 MeV/fm³ and in the case $m_u = m_d = 10$ MeV, it varies from 38 to 83 MeV/fm³.

§8. Compact stars

In this section we investigate the sequence of compact stars corresponding to the equation of state (EoS) in this model.

We consider a static, stationary and spherically symmetric perfect fluid for the stellar system. With these conditions, Einstein’s field equations yield the Tolman-Oppenheimer-Volkov (TOV) equation for hydrostatic equilibrium in general relativity:⁵⁾

$$-4\pi r^2 dP(r) = \frac{4\pi r^2 dr E(r)M(r)}{r^2} \cdot \frac{\left[1 + \frac{P(r)}{E(r)}\right] \left[1 + \frac{4\pi r^3 P(r)}{M(r)}\right]}{1 - \frac{2M(r)}{r}}, \tag{8.1}$$

where we denote the pressure at a radius r by $P(r)$, the energy density by $E(r)$, and the mass inside a radius r by $M(r)$:

$$M(r) = \int_0^r 4\pi r'^2 E(r') dr'. \tag{8.2}$$

We integrate the TOV equation employing the EoS shown in Fig. 11 from the center with a given central energy density until the pressure becomes zero. Doing so, a unique relationship among the mass, radius and central energy density is obtained.

Figures 14 and 15 show the sequence of compact stars corresponding to the EoS shown in Fig. 11. Figure 14 shows the relation between M/M_{sun} and the central energy density $E(0)$. It is seen that M/M_{sun} increases as $E(0)$ increases for $E(0) < 1300$ MeV/fm³. The maximum mass happens to be located at a value of $E(0)$ corresponding to $\mu \sim 600$ MeV (i.e., $\mu\bar{\rho} \sim 1$). If we increase $E(0)$ further away from the maximum mass point, the sequence goes into the unstable branch, i.e., the compact star mass decreases as $E(0)$ increases. Figure 15 displays the mass versus radius (R)

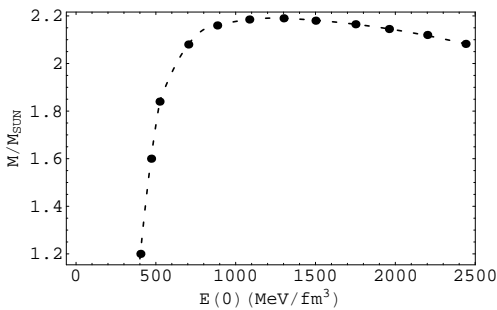


Fig. 14. The relation between the mass and the central energy density for compact stars corresponding to the EoS shown in Fig. 11.

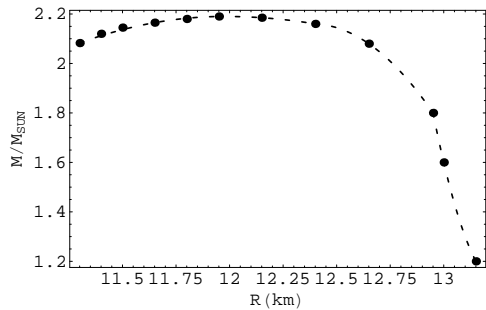


Fig. 15. Mass-radius relation for compact stars corresponding to the EoS shown in Fig. 11, where $M_{\text{sun}} = 1.99 \times 10^{33}$ g.

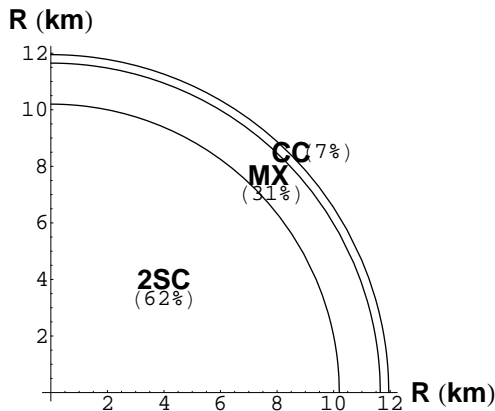


Fig. 16. The inner structure of the maximum mass compact star with $M = 2.19M_{\text{sun}}$. The volume fractions of the 2SC, MX and CC phases are 0.62, 0.31 and 0.07, respectively.

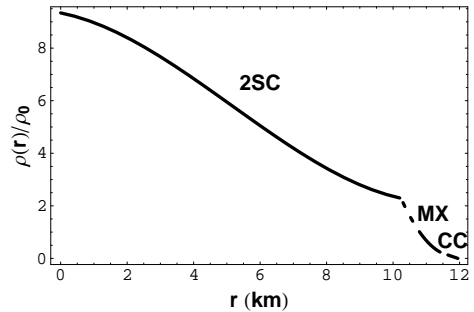


Fig. 17. Density profile of the same maximum mass star as shown in Fig. 16. Here, r is the distance from the center, and ρ_0 is the nuclear matter density.

relation. The maximum compact star mass of the sequence is about $2.19M_{\text{sun}}$ and its radius is about 12km. The values of $r - 2M(r)$ are positive everywhere inside compact stars.

Figures 16 and 17 show the interior structures of the maximum mass compact star with $E(0) = 1308 \text{ MeV/fm}^3$ ($\rho_B = 9.3\rho_0$). This compact star has mass of $M = 2.19M_{\text{sun}}$ and a radius of $R = 11.95 \text{ km}$. The compact star consists of three layers, i.e., the core, which is in the 2SC phase, from the center to $r = 10.2 \text{ km}$ ($\rho_B = 9.3\rho_0 - 2.67\rho_0$), the inner crust, which is in the mixed phase, between $r = 10.2 \text{ km}$ and 11.65 km ($\rho_B = 2.67\rho_0 - 0.13\rho_0$) and the outer crust, which is occupied by the CC phase, from $r = 11.65 \text{ km}$ to the stellar surface at $R = 11.95 \text{ km}$ ($\rho_B = 0.13\rho_0 - 0$). It is quite interesting that the mixed phase occupies 31% of the total volume of the star, although the range of the chemical potential for the mixed phase is not large.

§9. Conclusions

In the present study, we have investigated the phase structure of charge-neutral and β -equilibrated two-flavor (up and down) quark matter in the mean-field approximation. We have also investigated compact stars whose interiors are composed of two-flavor quark matter according to the equation of state. As the effective interaction, we used a μ -dependent instanton-induced interaction (μ -III), which arises from the μ -dependent quark zero mode. The μ -III is considered to be important in the region of low T and low to moderate μ that is relevant for compact stars. In addition to the locally electric charge-neutral pure chiral condensate (CC) and pure diquark condensate (2SC) phases, we have found that a new mixed phase, which is not a

locally but, rather, globally electric charge-neutral system, can be realized. The pure CC phase is realized between $\mu = 0$ and 293 MeV, and the mixing of the 2SC subphase starts at $\mu = 293$ MeV. The mixed phase consists of negatively charged CC and positively charged 2SC subphases. The volume fraction of the 2SC subphase increases monotonically from 0 at $(\mu, \mu_e) = (293 \text{ MeV}, 60 \text{ MeV})$ and reaches unity at $(\mu, \mu_e) = (320 \text{ MeV}, 212 \text{ MeV})$.

Several studies investigating the phase structure under the charge neutral condition have been carried out with NJL-type models, but their results are qualitatively different from the present one.^{1),2),6),9)-11),14)} The mixed phase that can be realized in some NJL-type models is a mixture of the normal quark matter (NQ : $\sigma = \Delta = 0$) subphase and the 2SC ($\Delta \neq 0$) subphase.^{9),12),36)} Furthermore, the phase structure depends on the effective coupling strengths for color-antitriplet quark pairs. In Refs. 11) and 14), for weak and intermediate coupling strengths ($K'/K \leq 0.75$), it is reported that no mixed phase is realized in the relevant region ($\mu \leq \sim 0.45 \text{ GeV}$). Only in the case of strong coupling ($K'/K \geq 1.0$) can the 2SC or NQ-2SC mixed phase be realized for $\mu \leq \sim 0.45 \text{ GeV}$. In one of the NJL-type model studies, it is reported that the charge-neutral 2SC phase is realized in a small μ -region between the color-flavor locking phase and the gapless 2SC phase.

In the μ -III model, a mixed phase and a charge-neutral 2SC phase is realized at $K'/K = 0.75$, and the particle number densities are continuous in the phase transitions. In addition, we have found that a finite current quark mass is advantageous in forming the mixed phase. A gapless 2SC phase does not exist at the baryon chemical potential that is relevant for compact star evolution.

The basic interactions between fermions in the μ -III model happen to be similar to those in the NJL-type models. However, there are some important differences between these two models, and these differences lead to discrepancies in the phase structures obtained with these two approaches. Here we discuss the differences between the two models.

I) In the μ -III model, unlike in the NJL-type models, there is no parameter like a coupling constant or UV momentum cutoff to be set so as to reproduce some physical quantities, for example, constituent quark mass and/or the pion decay constant. In the μ -III model, the effective coupling strength at each value of μ , which is inevitably μ -dependent, can be computed from the constraint on the effective coupling strength [Eq. (3.16) ; $\frac{N}{V} = \frac{\sigma^2}{4K} + \frac{\Delta^2}{4K'}$] with the coupled gap equations Eq. (3.24). The instanton density (N/V) and the average instanton size ($\bar{\rho}$) also have physical meanings directly connected to QCD. We employ the value of the gluon condensate from the lattice QCD calculation for the instanton density $\frac{N}{V}$.²⁶⁾ For the average instanton size $\bar{\rho}$, we adopt the result $\bar{\rho}(N/V)^{\frac{1}{4}} = \frac{1}{3}$ from the instanton liquid model calculation.²⁷⁾

II) We use the μ -dependent form factors derived without approximation from the quark zero mode function at finite μ in the instanton vacuum. While in the NJL-type models, simple form factors are introduced by hand, but they are μ independent.

III) It should be noted that the μ -III is originally a pre-exponential factor in the partition function. In return for raising the operator into the exponent, we have

an additional term [Eq. (2.12) ; $L_{\text{add}} \equiv N [\log(\frac{N}{2\lambda V}) - 1]$] and a constraint for the effective coupling strength $K(K')$ [Eq. (3.16) ; $\frac{N}{V} = \frac{\sigma^2}{4K} + \frac{\Delta^2}{4K'}$]. If we fix the values of $K(\propto \lambda)$ and N/V , the additional term L_{add} becomes constant, and thus, this term can be ignored. Indeed, in some III model studies, this strategy is used implicitly. As a consequence, a μ -independent form factor is required instead of the μ -dependent one, so as to realize chiral symmetry restoration at intermediate density. However, L_{add} is in fact crucial for phase structure. In Ref. 21) Carter and Diakonov investigated phase structure using the simple thermodynamic potential $\Omega = \Omega_{\text{free}} - \frac{N}{V} \log(\frac{N}{2\lambda V}) = \Omega_{\text{free}} - \frac{L_{\text{add}}}{V} - \frac{N}{V}$. The phase structure is determined by only the second term on the right-hand side. For the μ -III model, 1) the μ -dependent form factors, 2) L_{add} and 3) the constraint Eq. (3.16) are all necessary to realize a chiral phase transition at intermediate density. In addition, it is important to note that due to the constraint $\frac{N}{V} = \frac{\sigma^2}{4K} + \frac{\Delta^2}{4K'}$, the NQ($\sigma = \Delta = 0$) phase is not realized as long as III is effective. Thus in the μ -III model, the mixed phase consists of the CC and 2SC subphases. If we ignore these three important features, the μ -III model reduces to the NJL model. In this study, we have retained these three important features of the μ -III model, which originate from QCD.

We have investigated the upper limit of the surface tension η_{ul} , below which the mixed phase is favored over the locally neutral phases at a given μ , by assuming a crystalline structure with Wigner-Seitz cells for the mixed phase architecture. We find that the value of η_{ul} varies from several MeV/fm² to about 40 MeV/fm². In a recent study within the framework of the NJL model, the surface tension at the NQ-2SC interface is estimated to be at most a few MeV/fm² in the region corresponding to the mixed region in the μ -III model.^{9),30)} If this estimation is also valid in the μ -III model, the effects of the surface tension and the Coulomb force should be small enough that they do not affect the results qualitatively. Furthermore, by setting the value of the surface tension to 5 MeV/fm², we find that a Wigner-Seitz cell has a radius of order 10 fm. Accordingly, we believe that the mixed phase region may be homogeneously occupied by Wigner-Seitz cells of order 10 fm.

In the present model, the bag pressure (B) appears as the difference between the pressure of the CC and virtual NQ ($\sigma = \Delta = 0$) phases. At $\mu = T = 0$, we have $B^{\frac{1}{4}} \sim 0.25$ GeV. In addition, it is interesting that in the CC phase, the ratio n_d/n_u is almost the same as that in neutron matter.

The equation of state in the μ -III model is somewhat stiffer than those in the NJL-type and simple phenomenological bag models.^{11),14),20),37)} For example, in Ref. 14), it was found that $P \sim 100$ MeV/fm³ at $E = 500$ MeV/fm³ and $P \sim 300$ MeV/fm³ at $E = 1000$ MeV/fm³, while in this model, we have $P \sim 180$ MeV/fm³ at $E = 500$ MeV/fm³ and $P \sim 400$ MeV/fm³ at $E = 1000$ MeV/fm³. The gap Δ , which itself is a result of the strong coupling strength for a color anti-triplet bilinear, may have a large effect on equation of state (EoS) and hence on the mass-radius relationship of a compact star. As mentioned above, the value of Δ at each value of μ in the present model is a few times larger than that in the NJL type models and in the phenomenological bag model.^{11),14),37)} The large value of Δ may raise the pressure at each value of the energy density and hence stiffen the EoS of the

system. Therefore, the relatively heavy maximum compact star mass predicted by the present model may be a result of the large diquark gap Δ . For example, in Ref. 37), Alford and Reddy show that the maximum compact star mass increases as the gap Δ increases for $\Delta > 100$ MeV.

We have found that there are reasonable relations among the masses, radii and central energy densities for the compact stars in the μ -III model. The masses are of order M_{sun} , the radii are of order 10 km and the central energy densities are of order 10^{15} g/cm³. The maximum mass (M_{max}) of the sequence in this model is about $2.2M_{\text{sun}}$ and its radius is about 12 km. The compact star masses of the sequence in this model are somewhat heavier than the typical masses of observed radio pulsars, $1.35 \pm 0.04M_{\text{sun}}$.³⁸⁾

In general, a mass-radius relationship depends on the equation of state of the matter inside the compact star in question. The predicted masses of pure neutron stars do not exceed $2.0M_{\text{sun}}$.⁵⁾ The appearance of strangeness results in a reduction of the value of M_{max} for a compact star. Consequently, the maximum mass of a hyperon-mixed neutron star also does not exceed $2.0M_{\text{sun}}$.³⁹⁾ However, recently, Stairs et al. have estimated the mass of a pulsar (PSRJ0751+1807), which is a millisecond pulsar in a 6 hr orbit with a helium white dwarf secondary, by measuring the decay of its orbit due to the emission of gravitational radiation. The estimated mass of $M = 2.1 \pm 0.2M_{\text{sun}}$ is the largest recorded for a pulsar.⁴⁰⁾ This mass is comparable to M_{max} in the μ -III model. Taking into account the fact that the μ -III is important at low temperatures and low to moderate baryon densities, it is reasonable to conclude that compact stars in the μ -III model may provide a useful description of such relatively heavy compact star.

As seen in Fig. 8, the locally charge-neutral 2SC phase appears at about $2.67\rho_0$. As mentioned above, in other models such as NJL-type models, the locally charge-neutral 2SC phase is not realized in the relevant region. Thus μ -III gives a very different picture of the structure of the core of compact stars.

The new mixed phase spreads over only a few kilometers as a middle layer inside compact stars. However, in some compact stars, such middle layers occupy the largest volumes inside the compact stars. For example, in the case $E(0) = 0.84 \times 10^{15}$ g/cm³, the volume fractions of the 2SC core, MX layer and CC layer are 0.4, 0.46 and 0.14, respectively. Therefore, existence of the newly discovered mixed phase as well as the 2SC phase inside a compact star could be relevant in some phenomena, e.g., glitch and transport properties.

Acknowledgements

The authors thank Dr. N. Ishii for useful comments and discussions.

Appendix A

— The Fourier Transform of the Quark Zero Mode Function —

In this appendix we present the Fourier transform of the quark zero mode at finite chemical potential.²¹⁾

The quark zero mode solution can be written as

$$\Psi_{(0)}^{\alpha i}(x-z, \mu) = -i \left[\int \frac{d^4 p}{(2\pi)^4} e^{ip(x-z)} \phi_\nu(p, \mu) \gamma^\nu \frac{1 + \gamma_5}{2} \right]_{ij} \cdot \frac{\epsilon^{j\beta}}{\sqrt{2}} \cdot U_\beta^\alpha, \quad (\text{A}\cdot 1)$$

where i and j are flavor indices, α and β are color indices and U represents the color orientation matrix.

The Fourier transforms $\phi_\nu(p, \mu)$ are given by

$$\begin{aligned} \phi_i(\mathbf{p}, p_4, \mu) &= p_i \cdot \phi(|\mathbf{p}|, p_4, \mu) \quad (i = 1 - 3), \\ \phi_4(|\mathbf{p}|, p_4, \mu) &= \frac{\pi \bar{\rho}^2}{4|\mathbf{p}|} \{ (2|\mathbf{p}| - \mu - ip_4)[(2p_4 + i\mu)f_{1-} + i(|\mathbf{p}| - \mu - ip_4)f_{2-}] \\ &\quad + (|\mathbf{p}| + \mu + ip_4)[(2p_4 + i\mu)f_{1+} - i(|\mathbf{p}| + \mu + ip_4)f_{2+}] \}, \end{aligned} \quad (\text{A}\cdot 2)$$

where

$$\begin{aligned} \phi(|\mathbf{p}|, p_4, \mu) &= \frac{\pi \bar{\rho}^2}{4|\mathbf{p}|^2} \left\{ (2|\mathbf{p}| - \mu)(|\mathbf{p}| - \mu - ip_4)f_{1-} + (2|\mathbf{p}| + \mu)(|\mathbf{p}| + \mu + ip_4)f_{1+} \right. \\ &\quad + [2(|\mathbf{p}| - \mu)(|\mathbf{p}| - \mu - ip_4) - \frac{1}{|\mathbf{p}|}(\mu + ip_4)(p_4^2 + (|\mathbf{p}| - \mu)^2)]f_{2-} \\ &\quad \left. + [2(|\mathbf{p}| + \mu)(|\mathbf{p}| + \mu + ip_4) + \frac{1}{|\mathbf{p}|}(\mu + ip_4)(p_4^2 + (|\mathbf{p}| + \mu)^2)]f_{2+} \right\}. \end{aligned} \quad (\text{A}\cdot 3)$$

Here we have introduced the functions

$$f_{1\pm} = \frac{1}{z_\pm} [I_1(z_\pm)K_0(z_\pm) - I_0(z_\pm)K_1(z_\pm)], \quad (\text{A}\cdot 4)$$

$$f_{2\pm} = \frac{1}{z_\pm^2} I_1(z_\pm)K_1(z_\pm), \quad (\text{A}\cdot 5)$$

where I_0, I_1, K_0 and K_1 are the modified Bessel functions and the arguments z_\pm are given by $z_\pm = \frac{1}{2}\bar{\rho}\sqrt{p_4^2 + (|\mathbf{p}| \pm \mu)^2}$.

References

- 1) M. Alford, *Annu. Rev. Nucl. Part. Sci.* **51** (2001), 131.
- 2) M. Alford, *Prog. Theor. Phys. Suppl. No.* 153 (2004), 1.
- 3) M. Alford, K. Rajagopal and F. Wilczek, *Nucl. Phys. B* **537** (1999), 443.
- 4) N. Itoh, *Prog. Theor. Phys.* **44** (1970), 291.
- 5) N. K. Glendenning, *Compact stars: Nuclear physics, Particle Physics and General Relativity* (Springer, New York, London, 2000).
- 6) I. Shovkovy and M. Huang, *Phys. Lett. B* **564** (2003), 205.
- 7) N. Iwamoto, *Phys. Rev. Lett.* **44** (1980), 1637.
- 8) K. Yamaguchi, M. Iwasaki and O. Miyamura, *Prog. Theor. Phys.* **107** (2002), 117.
- 9) A. W. Steiner, S. Reddy and M. Prakash, *Phys. Rev. D* **66** (2002), 094007.
- 10) F. Neumann, M. Buballa and M. Oertel, *Nucl. Phys. A* **714** (2003), 481.
- 11) H. Grigorian, D. Blaschke and D. N. Aguilera, *Phys. Rev. C* **69** (2004), 065802.
- 12) D. Blaschke, S. Fredriksson, H. Grigorian, A. M. Öztaş and F. Sandin, *Phys. Rev. D* **72** (2005), 065020.
- 13) D. N. Aguilera, D. Blaschke, M. Buballa and V. L. Yudin, *Phys. Rev. D* **72** (2005), 034008.

- 14) D. N. Aguilera, D. Blaschke and H. Grigorian, Nucl. Phys. A **757** (2005), 527.
- 15) S. B. Rüster, V. Werth, M. Buballa, I. Shovkovy and D. H. Rischke, Phys. Rev. D **72** (2005), 034004.
- 16) I. Shovkovy and M. Huang, Phys. Lett. B **564** (2003), 205.
- 17) M. Alford, C. Kouvaris and K. Rajagopal, Phys. Rev. Lett. **92** (2004), 222001.
- 18) H. Abuki, M. Kitazawa and T. Kunihiro, Phys. Lett. B **615** (2005), 102.
- 19) M. Buballa, F. Neumann, M. Oertel and I. Shovkovy, Phys. Lett. B **595** (2004), 36.
- 20) M. Alford, M. Braby, M. Paris and S. Reddy, Astrophys. J. **629** (2005), 969.
- 21) G. W. Carter and D. Diakonov, Phys. Rev. D **60** (1999), 016004.
- 22) H. Kiuchi and M. Oka, Prog. Theor. Phys. **114** (2005), 813.
- 23) M. Alford, K. Rajagopal and F. Wilczek, Phys. Lett. B **422** (1998), 247.
- 24) J. Berges and K. Rajagopal, Nucl. Phys. B **538** (1999), 215.
- 25) G. 't Hooft, Phys. Rev. D **14** (1976), 3432.
- 26) M. Chu, J. Grandy, S. Huang and J. Negele, Phys. Rev. D **49** (1994), 6039.
- 27) D. Diakonov and V. Petrov, Phys. Lett. B **147** (1984), 351.
- 28) M. A. Shifman, A. I. Vainshtein and V. I. Zakharov, Nucl. Phys. B **163** (1980), 46.
- 29) C. G. Callan, R. Dascen and D. J. Gross, Phys. Rev. D **17** (1978), 2717.
- 30) S. Reddy and G. Rupak, Phys. Rev. C **71** (2005), 025201.
- 31) C. A. de Carvalho, Nucl. Phys. B **183** (1981), 182.
- 32) G. Baym, H. Bethe and C. Pethick, Nucl. Phys. A **175** (1971), 225.
- 33) D. Ravenhall, C. Pethick and J. Wilson, Phys. Rev. Lett. **50** (1983), 2066.
- 34) N. K. Glendening and S. Pei, Phys. Rev. C **52** (1995), 2250.
- 35) D. Voskresensky, M. Yasuhira and T. Tatsumi, Phys. Lett. B **541** (2002), 93.
- 36) I. Shovkovy, M. Hanauske and M. Huang, Phys. Rev. D **67** (2003), 103004.
- 37) M. Alford and S. Reddy, Phys. Rev. D **67** (2003), 074024.
- 38) S. E. Thorsett and D. Chakrabarty, Astrophys. J. **512** (1999), 288.
- 39) T. Takatsuka, Prog. Theor. Phys. Suppl. No. 156 (2004), 84.
- 40) D. J. Nice, E. M. Splaver, I. H. Stairs, O. Löhmer, A. Jessner, M. Kramer and J. M. Cordes, astro-ph/0508050.